catalysts

MDPI

Article

Physical Origin of Diminishing Photocatalytic Efficiency for Recycled TiO_2 Nanotubes and Ag-Loaded TiO_2 Nanotubes in Organic Aqueous Solution

Theint Hay Mar Wint [1], Michael F. Smith [2], Narong Chanlek [3], Fuming Chen [4], Than Zaw Oo [5] and Prayoon Songsiriritthigul [2,6,*]

1 Materials Research Laboratory, Department of Physics, University of Mandalay, Mandalay 05032, Myanmar; theinthaymarwint@gmail.com
2 Research Network NANOTEC–SUT on Advanced Nanomaterials and Characterization, School of Physics, Suranaree University of Technology, Nakhon Ratchasima 30000, Thailand; mfsmith@g.sut.ac.th
3 Synchrotron Light Research Institute, Muang, Nakhon Ratchasima 30000, Thailand; narong@slri.or.th
4 Guangdong Provincial Key Laboratory of Quantum Engineering and Quantum Materials, South China Normal University, Guangzhou 510006, China; fmchen@m.scnu.edu.cn
5 Universities' Research Centre, University of Yangon, Yangon 11041, Myanmar; thanzawoo@uy.edu.mm
6 Thailand Center of Excellence in Physics, MHESRI, Bangkok 10400, Thailand
* Correspondence: py.song@sut.ac.th; Tel.: +66-8-9845-9032

Received: 27 May 2020; Accepted: 1 July 2020; Published: 3 July 2020

Abstract: Arrays of titania nanotubes (TiO_2NTs) were developed by electrochemical anodization and doped with silver on their surface by photodeposition to achieve TiO_2NTs/Ag. It is found that only anatase TiO_2NTs were formed, with the preferential growth direction perpendicular to the titanium substrate, and with the length and diameter of ~2 μm and 90–120 nm, respectively. The presence of Ag on the surface of TiO_2NTs was also confirmed. The TiO_2NTs and TiO_2NTs/Ag were used as photocatalysts to decolorize the methylene blue (MB) aqueous solution. The photodegradation efficiency (PDE) is as high as 83% for TiO_2NTs and 98% for TiO_2NTs/Ag photocatalysts. This work focused on the investigation of the stability and recyclability of these photocatalysts in terms of efficiency and its physical origin by surface analysis using X-ray photoelectron spectroscopy (XPS). It is found that PDE diminishes from 83% to 76% in TiO_2NTs upon eight recycling runs and from 98% to 80% in TiO_2NTs/Ag upon six recycling runs. The XPS analysis revealed that the physical origin of diminishing efficiency is the carbon contamination on the surface of recycled TiO_2NTs and a combination of carbon contamination and Ag leaching in recycled TiO_2NTs/Ag.

Keywords: water treatments; photocatalysts; TiO_2 nanotubes; Ag nanoparticles; diminishing efficiency; XPS; carbon contamination

1. Introduction

Titania nanotubes (TiO_2NTs) continue to attract attention from researchers interested in photocatalytic degradation of organic pollutants in water. The parent material TiO_2 is stable and inexpensive and the TiO_2NTs have several physical properties ideal for photodegradation: their ordered porous architecture, with a unidirectional electrical channel, large surface area, and long charge carrier lifetime [1–7]. Two well-known drawbacks of using TiO_2 in solar photocatalysis applications are: (i) its wide band gap, which requires UV frequencies to initiate the charge transfer mechanism and (ii) the rapid electron hole recombination rate of photogenerated carriers [8–12]. The main strategy

used to overcome these challenges is to dope TiO_2, perhaps with noble metals like Ag or Au [13–16]. Isolated impurities can provide absorbing defect states that may improve the problem (i). These localized states can also relieve problem (ii) by trapping one carrier while the other escapes. Of course, a reduction of the recombination rate can only prevent losses from a small initial carrier population while the band gap remains in the UV range. There is an enormous literature describing the effects of metallic, and nonmetallic, dopants on the optical and electrical properties of composite TiO_2 [17–20].

The results of Ag loading in TiO_2 have been particularly promising for photocatalytic applications. An optimized level of Ag loading in TiO_2 can dramatically increase photodegradation efficiency [21–24]. Part of this increase can be explained by the idea that photoexcited electrons trapped near isolated Ag defects can transfer to the sample surface and initiate the desired chemical reaction before being lost to recombination. However, the large enhancement is mainly attributed to a different physical effect, possible only when the Ag ions agglomerate into nanostructures within the semiconductor host. Light in the visible range can excite a plasmon on the surface of the metal nanoparticle, dubbed a local surface plasmon resonance or LSPR. This excitation in the metal induces a carrier population in the surrounding TiO_2, making a large increase of the photocatalytic rate possible.

The two most likely ways for the LSPR in the Ag to result in a population of free carriers in TiO_2 is by direct charge transfer and local field enhancement. In the first case, electrons excited at the metallic surface by the LSPR can hop to the conduction band in TiO_2 (or electrons in the semiconductor valence band can hop into empty states in the metal that were vacated during the LSPR). In the second case, the LSPR produces a strong local electric field that can drive carriers across the semiconductor band gap [25–27]. Either way, the potential enhancement to photocatalytic rates under solar radiation (which contains a relatively small fraction of UV photons) and other visible light sources is enormous.

The silver nanoparticle loaded TiO_2NTs, which realize the LSPR, have recently been incorporated into real-life photocatalytic applications [28–32]. The stability and recyclability of catalysts in these devices are needed for industrial viability. Ideally, the catalysts should withstand repeated reactions without a significant loss in efficiency. However, in many TiO_2-based photocatalytic devices, including silver-loaded TiO_2NTs, a drop in efficiency with the number of recycling runs has been reported [33–38]. To the best of our knowledge, there is no detailed study about the main factors responsible for the loss of photocatalytic efficiency with repeated cycles in TiO_2NTs and silver nanoparticle loaded analogs.

Below we track photocatalytic performance over several cycles and investigate the likely mechanism for its decline. Since experiments are done under UV light, which can excite carriers across the native band gap, we do not address any decline that might result from a reduction in the initial carrier population. Rather, we aim to isolate the part of the decline that still occurs when excited carriers are abundant. It would seem necessary to disentangle the two potential causes for the observed drop in photocatalytic efficiency in this way.

We present a study primarily focused on an exploration of the physical origin of diminishing photocatalytic efficiency of TiO_2NTs and TiO_2NTs/Ag after repeated recycling runs. First, we characterize the structural and optical properties of TiO_2NTs/Ag. Particularly, we observe the formation of a visible absorption band, attributed to the LSPR, with increasing concentration of Ag. This band emerges abruptly: a 0.1 M concentration of Ag has no effect on visible absorption of the titania nanotube but for concentrations above 0.5 M, the broad band is present and dominates visible absorbance. The appearance of sample nanostructure, inspected by scanning electron microscopy (SEM), exhibits a similar qualitative difference between the 0.1 M samples and those of higher concentration. We attribute it to a change in Ag morphology, with silver nanoparticles (AgNPs) forming above a critical Ag concentration. The efficiency of these catalysts in degrading the organic pollutant, methylene blue, in aqueous solution was then measured under UV light irradiation. The optimal Ag content of TiO_2NTs for photocatalytic performance is identified and discussed in relation to the observed nanostructure. Finally, we used X-ray photoelectron spectroscopy (XPS) on the optimally loaded sample to track the change in the local structure surrounding each atomic species in the sample

that occurs with repeated catalytic cycles. In this way, we identify the most likely mechanism for diminishing photocatalytic performance.

2. Results and Discussions

2.1. Physicochemical Properties of TiO_2NTs and TiO_2NTs/Ag

Figure 1 shows the field emission scanning electron microscopy (FESEM) micrographs of TiO_2NTs and TiO_2NTs/Ag-0.1 M, -0.5 M and 1.0 M samples. The TiO_2NT arrays are apparently well-ordered. The inner diameter of the average nanotube is 90–120 nm and its average length is ~2 μm. Inspecting Figure 1, there is a qualitative difference between the structural characteristics of TiO_2NTs and TiO_2NTs/Ag-0.1 M, on the one hand, and those of TiO_2NTs/Ag-0.5 M and 1.0 M on the other. That is, the smallest Ag concentration of 0.1 M does not have any apparent effect on the morphology of the titania nanotubes. At higher concentrations, there is a clear indication of silver deposition on the surface of TiO_2NTs. This is relevant to the putative LSPR effect discussed above. If Ag atoms are incorporated as isolated impurities (isolated atoms or very small clusters of atoms), they will modify optical properties mainly via localized states in the band gap. However, if the silver forms clusters large enough then it can support surface plasmons excitable by visible light. While we have not established the actual morphology of the Ag in the TiO_2NTs, the SEM images should be considered alongside the visible absorbance shown below.

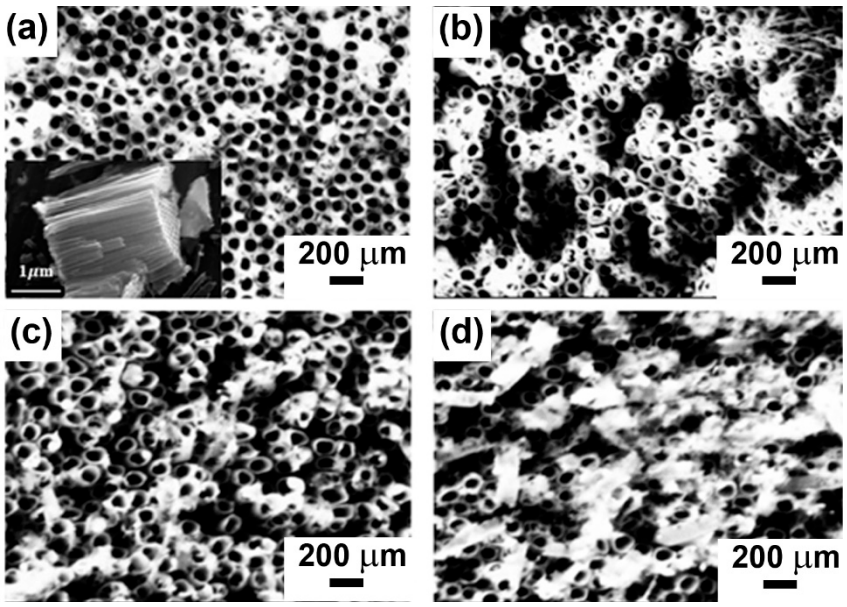

Figure 1. FESEM micrographs of (**a**) TiO_2NTs, (**b**) TiO_2NTs/Ag-0.1 M, (**c**) TiO_2NTs/Ag-0.5 M and (**d**) TiO_2NTs/Ag-1.0 M. Inset in (**a**): the cross-section SEM image showing the length of TiO_2NTs.

The crystalline phase of TiO_2NTs and TiO_2NTs/Ag annealed at 500 °C was examined using X-ray diffraction (XRD). In the XRD profiles (Figure 2), the diffraction peaks at 25.2°, 37.8°, 47.9°, 53.8°, 54.9° and 62.9° could be indexed to (101), (004), (200), (105), (211) and (204) crystalline planes of the anatase TiO_2. For nanoparticles, anatase is usually the most stable of the three possible TiO_2 crystal structures—and is slightly advantageous in charge separation applications because of its surface chemistry. There was no significant change in the crystal structure that occurred with Ag concentration. While the FESEM indicated that Ag was incorporated in the form of metallic Ag, no Ag crystal peaks were detected in the XRD patterns of TiO_2NT/Ag-0.1 M, -0.5 M and -1.0 M samples. The deposited Ag is likely too small and few in number to be detected.

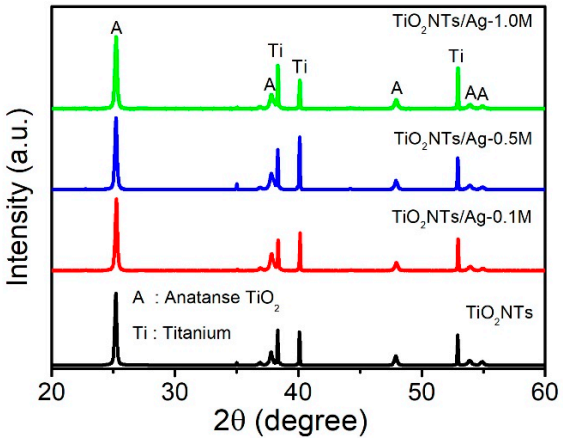

Figure 2. XRD patterns of TiO_2NTs and TiO_2NTs/Ag-0.1 M, -0.5 M and -1.0 M.

To verify the presence of AgNPs on TiO_2NTs, the UV-vis diffuse reflectance spectra for TiO_2NTs, TiO_2NTs/Ag-0.1 M, -0.5 M and -1.0 M were acquired and shown in Figure 3. We see similar optical properties for the 0.1 M sample and pure TiO_2. The lowest concentration of Ag had no effect on visible light absorption. However, for the TiO_2NTs/Ag-0.5 M and -1.0 M samples, a broad absorption peak centered between 450 and 500 nm emerges. This peak is attributed to the local surface plasmon resonance (LSPR) of AgNPs. The data again suggests that there is a qualitative difference between samples with an Ag concentration as low as 0.1 M compared to those with a concentration above 0.5 M. Our results strongly imply that the AgNPs only form above some minimum concentration of Ag. Below this concentration, we expect that the silver is deposited in a different form, perhaps as isolated impurities. If the associated impurity levels were mainly near band edges, they would have no effect on visible absorbance, which appears to be the case for 0.1 M Ag. Previous studies [39,40] have addressed the size-dependence of the visible absorbance spectra for AgNPs. A broad visible band is present for AgNPs as small as 3 nm (though its shape depends on both the size and shape of the nanoparticle). The presence of nanoparticles of this size would cause a dramatic increase in visible absorption, as is clearly seen for concentrations above 0.5 M.

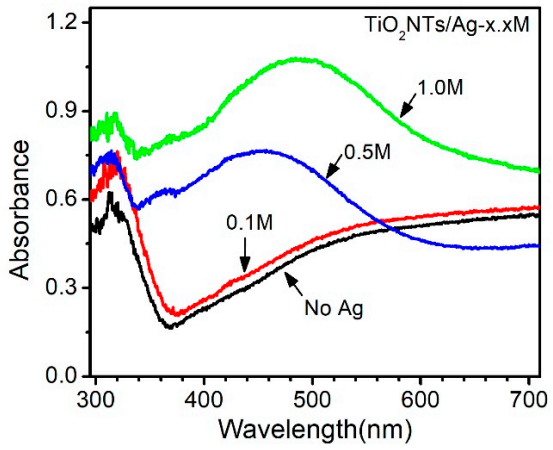

Figure 3. UV-vis diffuse reflectance spectra of TiO_2NTs, TiO_2NTs/Ag-0.1 M, -0.5 M and -1.0 M samples.

The surface composition of TiO_2NTs and the oxidation states of Ag on the surface of TiO_2NTs were investigated by XPS. Figure 4a shows the wide-scan XPS spectra in which titanium, oxygen, carbon, nitrogen and silver (in TiO_2NTs/Ag) are detected. That is, we investigate the local structure of all native ions, the Ag dopants, and additional species present due to adventitious contamination on the surface. A tiny amount of nitrogen may come from electrolyte (ammonium fluoride solution).

The high-resolution XPS spectra of Ag 3d, Ti 2p and O 1s are depicted in Figure 4. The XPS spectra of Ag 3d in Figure 4c reveal two prominent peaks with 6 eV spin–orbit separation that are centered around 374.2 eV and 368.2 eV. These correspond to Ag $3d_{5/2}$ and Ag $3d_{3/2}$, respectively. This is the characteristic of metallic silver (Ag^0) [41] indicating that the Ag^+ ions are reduced to metallic silver (Ag^0) on TiO_2NTs during the UV light irradiation. The intensities of the Ag 3d peaks understandably increased with increasing Ag concentration. In the XPS spectra of Ti 2p and O 1s in Figure 4a,b, two peaks of Ti $2p_{3/2}$, Ti $2p_{1/2}$ and one peak of O 1s are observed at the binding energy of 458.5 eV, 464.3 eV and 530.0 eV respectively. The difference in binding energies of Ti $2p_{3/2}$ and Ti $2p_{1/2}$ is 5.8 eV, implying that Ti has a tetravalent state in TiO_2NTs [21,23]. The measured binding energies of Ti $2p_{3/2}$ peak, Ti $2p_{1/2}$ peak and O 1s peak are in good agreement with the usual results for anatase TiO_2 [42].

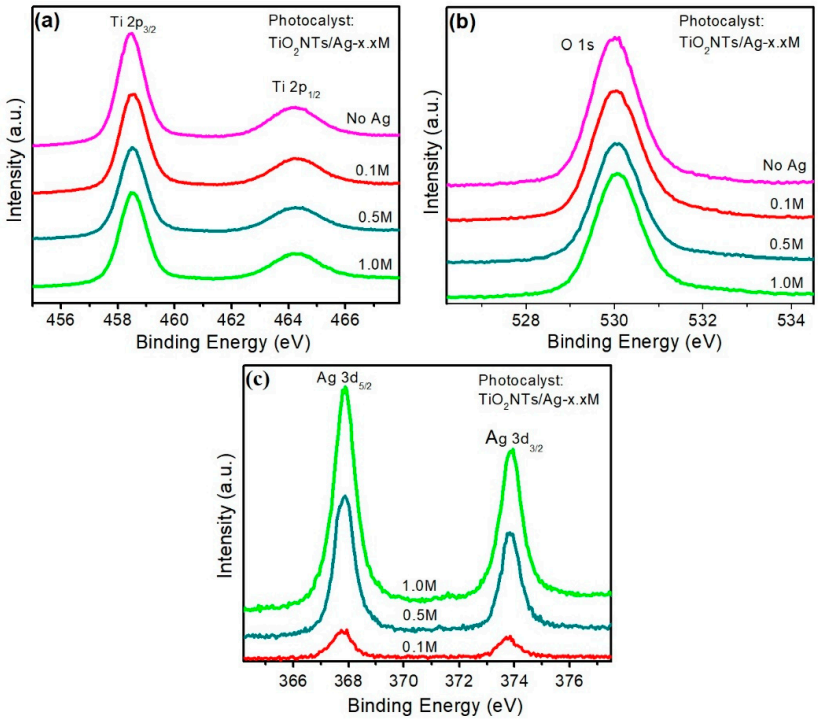

Figure 4. Fine-scan XPS spectra of (**a**) Ti 2p (**b**) O 1s and (**c**) Ag 3d.

Table 1 lists the surface Ti, O, C, N and Ag atomic concentrations determined by XPS peak intensities for all samples. The XPS results verified the presence of Ag on the surface of all Ag-loaded TiO_2NTs samples. Indeed, the amount of Ag on the surface, as indicated by XPS, is approximately proportional to the total concentration of Ag throughout the sample. This means that Ag is always present on the nanotube surfaces, but that at lower concentrations it does not modify structural and optical characteristics of the samples. This is again consistent with our claim that the qualitative difference in optical absorbance between samples with 0.1 M Ag compared to those of higher Ag content indicates a change in Ag morphology, with AgNPs present in the latter.

Table 1. The surface Ti, O, C, N and Ag atomic concentrations determined by XPS for TiO_2NTs and TiO_2NTs/Ag samples.

Samples	Ti at.%	O at.%	C at.%	N at.%	Ag at.%
TiO_2NTs	29.64	59.54	9.38	1.44	-
TiO_2NTs/Ag-0.1 M	28.54	58.97	11.87	-	0.62
TiO_2NTs/Ag-0.5 M	27.11	57.67	11.89	0.52	2.81
TiO_2NTs/Ag-1.0 M	25.81	56.53	12.98	0.43	4.25

2.2. Photodegradation Efficiency of TiO_2NTs and TiO_2NTs/Ag Photocatalysts

The propensity for the TiO_2NTs and TiO_2NTs/Ag to degrade the organic pollutant, methylene blue (MB), is considered next. Figure 5a shows the photodegradation efficiency (PDE) of TiO_2NTs and TiO_2NTs/Ag over the UV irradiation time of 1 to 5 h. The PDE is enhanced by the addition of Ag, and begins to increase immediately. That is, the TiO_2NTs/Ag-0.1 M sample exhibits a significantly larger PDE than the pure TiO_2. With increasing Ag loading, the PDE first increases, being largest for TiO2NTs/Ag-0.5 M, then decreases. This limited data set indicates that the optimal Ag concentration for ultraviolet photodegradation of MB lies between 0.1 and 1.0 M. For a given irradiation time of 5 h, the PDE of TiO_2NTs/Ag-0.1 M, -0.5 M and -1.0 M are respectively 89%, 98% and 87% as compared to a value of 83% for pure TiO_2NTs. It is noted that when no photocatalyst was used, blanc experiments, the measured photodegradation efficiency was relatively low (4%, 7%, 12%, 15% and 17% for 1-, 2-, 3-, 4- and 5-h of UV irradiation.)

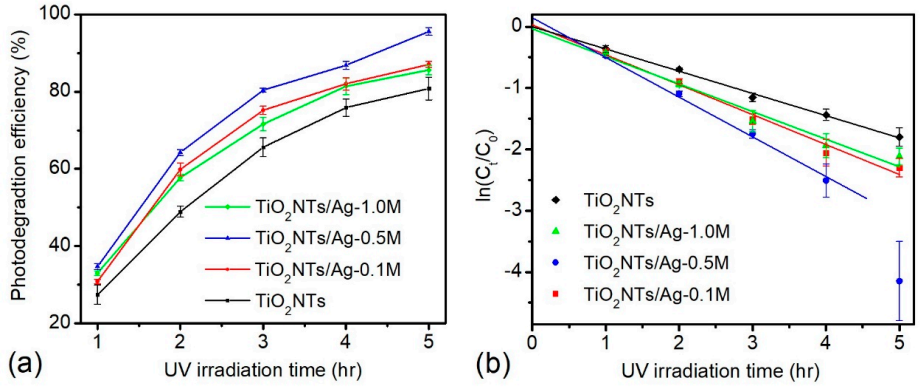

Figure 5. Plots of (**a**) photodegradation efficiency and (**b**) ln (Ct/Co) against UV irradiation time for TiO_2NTs and TiO_2NTs/Ag-0.1 M, -0.5 M and 1.0 M catalysts.

Since the experiments were carried out under UV irradiation, the enhanced absorption of visible light, due to the LSPR, is not responsible for the improved PDE. Indeed, the increase in PDE occurred even for the AgNPs-0.1 M sample, which showed no evidence for silver nanoparticles and no difference in optical properties from those of pure TiO_2. Rather, the improved PDE may be attributed to reduced charge recombination rate occurring in the presence of Ag loading [43–45]. A decrease in PDE with a further increase of Ag (1.0 M) is ascribed to an increased agglomeration of Ag nanoparticles on the TiO_2 surface which blocks the UV light (less photoactivity) and decreases an effective area for photocatalytic reaction [46,47]. The plots of $\ln(C_t/C_0)$ versus time, shown in Figure 5b, exhibit approximately linear behavior, indicating first-order kinetics. The degradation rate constant (k) is found to be 0.0060 min^{-1}, 0.0081 min^{-1}, 0.0112 min^{-1} and 0.0075 min^{-1} for TiO_2NTs, TiO_2NTs/Ag-0.1 M, -0.5 M and -1.0 M, respectively. It is noted that the degradation rate constant for TiO_2NTs/Ag-0.5 M was determined for the UV irradiation only up to 4 h.

2.3. Physical Origin of Diminished Efficiency in Recycled TiO_2NTs and TiO_2NTs/Ag Photocatalysts

Recycling experiments, in which several photodegradation trials were performed successively, were carried out for these systems. For each trial, an initial concentration of 12mg/l of MB with pH = 1 was used. Figure 6 shows the photodegradation efficiencies of TiO_2NTs and TiO_2NTs/Ag-0.5 M for these recycling runs. It is found that the photodegradation efficiency of TiO_2NTs dropped from 83% to 76% after eight cycles while that of the TiO_2NTs/Ag-0.5 M decreased from 98% to 80% after six cycles. Two plausible explanations for the diminishing photodegradation efficiency upon recycling are (i) carbon enrichment on the surface of the photocatalysts and (ii) Ag depletion. Central to the present work is an effort to identify which mechanism is more important. Since XPS is a surface-sensitive technique for chemical analyses, it is ideal for addressing this question.

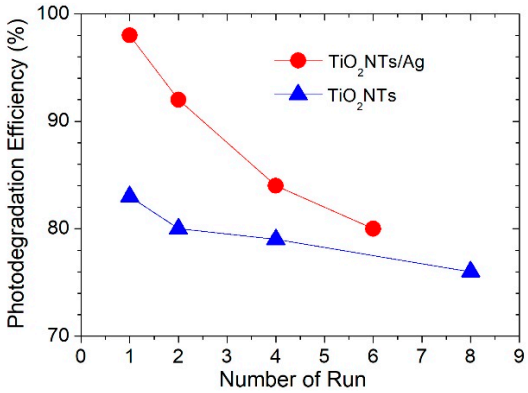

Figure 6. Photodegradation efficiency of TiO_2NTs (blue triangle) and TiO_2NTs/Ag (red circle) photocatalysts for degradation of MB.

Figure 7 depicts the XPS spectra and atomic concentration of Ti 2p, O 1s and C 1s and for fresh and recycled TiO_2NTs photocatalysts. The characteristic peak positions of Ti $2p_{3/2}$, Ti $2p_{1/2}$ and O 1s are the same for all trials. This suggests that there is no change in the valence state of these ions. The photoelectron signals of C 1s originated from different carbon species adsorbed on the samples. These signals contribute broad peaks shown in Figure 7c. The atomic concentrations of Ti, O and C deduced from the XPS spectra are given Figure 7d. It is noted that a small amount of nitrogen, less than a few at %, was also detected and not shown in the figure. As shown in Figure 7d, the atomic ratio between Ti and O is not 1:2. There is additional oxygen coming from surface contaminants. The obvious changes from the fresh to recycled TiO_2NT samples are observed in the XPS spectra of C 1s. The peak associated with C increases rapidly with cycle count. It is well-known that the XPS C1s spectrum for organic contaminants typically has C–C, C–O–C and O–C=O components with peak positions at 284.8, 286.0 and 288.5 eV, respectively.

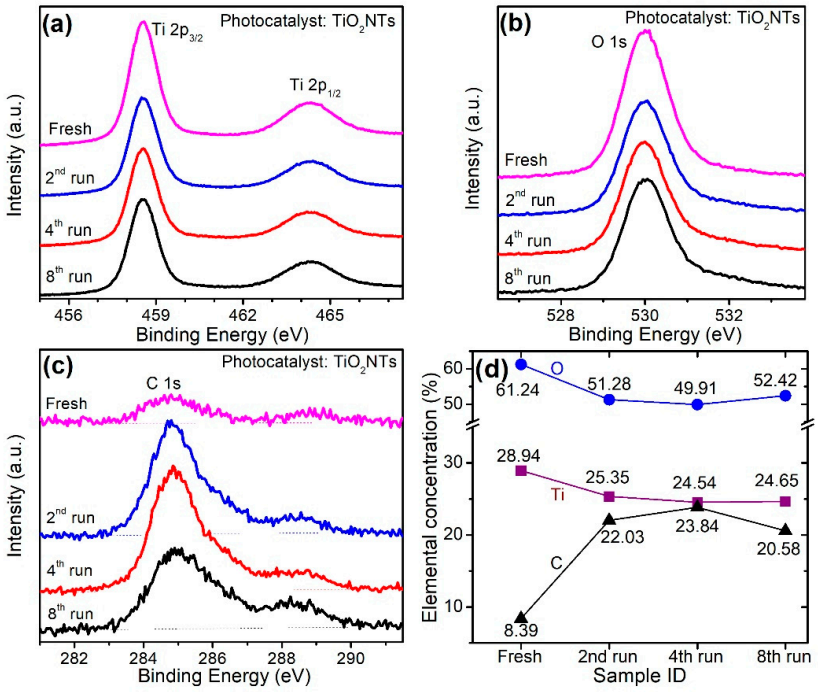

Figure 7. Fine-scan XPS spectra of (**a**)Ti 2p, (**b**) O 1s and (**c**) C 1s taken from recycled TiO_2NTs photocatalysts. (**d**) Ti, O, and C atomic concentrations determined by XPS for recycled TiO_2NTs catalyst (up to 8th run).

The carbon measured by XPS from the fresh TiO_2NTs sample was found to be about 8 at %. This carbon is the typical contamination on the surface of the sample. After two runs of the photocatalysis reaction, the amount of detected carbon increases by a factor of three. It should be noted that the sample was rinsed in water and dried under air blow after each photocatalysis trial. The amount of carbon did not change significantly after the first few runs: the amount of C was approximately the same after four and eight runs than detected after two runs. The additional carbon detected after two photodegradation cycles is likely that of CO_2 and other products of a complete photocatalytic oxidation process. This explains the increase of the intensity of C 1s photoelectrons at binding energies of 286.0 and 288.0 eV, due to C–O–C and O–C=O components, respectively. Given that the large increase in C contaminants, seen during the first two photodegradation cycles, coincides with the significant drop in PDE, there is an indication that the decline in the performance of TiO_2NTs as a photocatalyst results from carbon contamination on the surface. It is speculated that among several possible sources of carbon contamination, hydrocarbon adsorption (getting air-exposed) within recycling experiments and carbonate precipitation/MB sedimentation during photocatalytic reactions most likely contributed to surface carbon contamination in our samples.

Figure 8 shows the XPS spectra of Ti 2p, O 1s, Ag 3d and C 1s for fresh and recycled TiO_2NTs/Ag-0.5 M photocatalysts. There are no observable changes in the oxidation state of Ti and O over serval recycling runs. From the XPS spectra, the surface atomic concentrations of Ti, O, Ag and C in fresh and recycled TiO_2NTs/Ag photocatalysts are calculated and plotted in Figure 9. A striking feature is the rapid reduction of Ag concentration. After the 6th run, AgNPs could not be detected. The diminishing Ag concentration may be due to leaching of AgNPs from the surface of TiO_2NTs since the samples were rinsed with water and dried under air blow after each cycle. It is interesting to point out that the increase in carbon did not begin until the AgNPs were stripped from the samples. Once the Ag was removed, the bare TiO_2NTs experienced the same rapid accumulation of carbon contaminants that was seen in Figure 7. Obviously, as the Ag was stripped from the samples, the photodegradation capability of TiO_2NTs/Ag approached that of TiO_2NTs, which is seen in Figure 6.

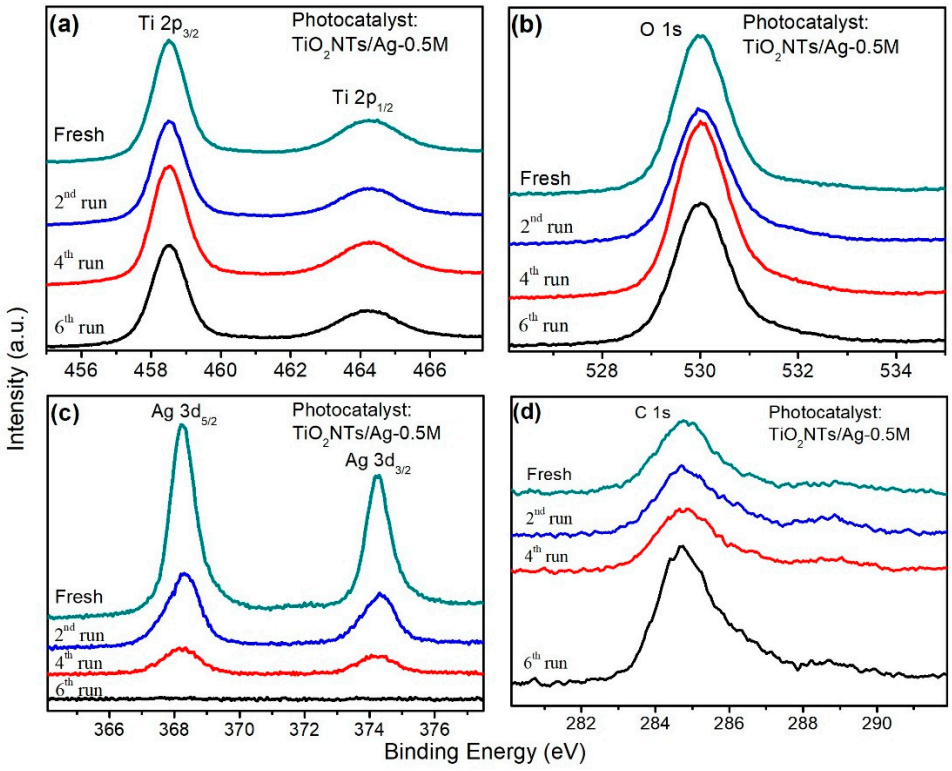

Figure 8. Fine-scan XPS spectra of (**a**) Ti 2p, (**b**) O 1s, (**c**) Ag 3d and (**d**) C 1s taken from fresh and recycled TiO_2NTs/Ag-0.5 M photocatalyst.

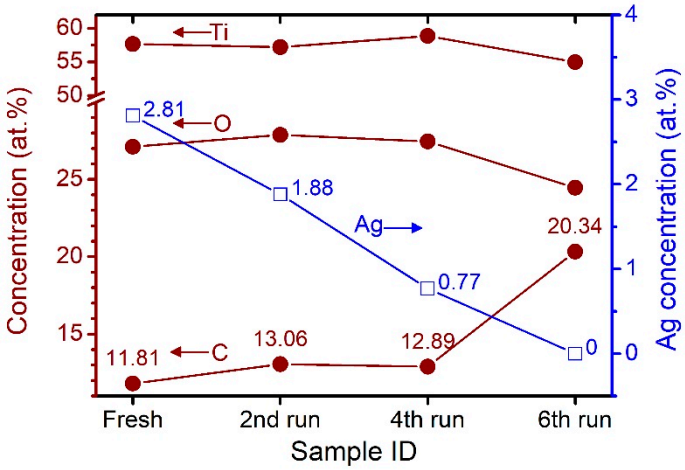

Figure 9. Ti, O, Ag, and C atomic concentrations determined by XPS for fresh and recycled TiO_2NTs/Ag catalysts (up to 6th run).

3. Materials and Methods

3.1. Development of TiO_2NTs and TiO_2NTs/Ag Samples

Titanium foils (area—2.5 cm × 2.0 cm, thickness—0.02 cm, purity 99.7%) were ultrasonically cleaned with acetone, ethanol and isopropanol for 10 min each. They were rinsed with distilled water and dried under air blow. The titanium dioxide nanotube (TiO_2NT) arrays were developed on the Ti base by electrochemical anodization. The anodization process was carried out with magnetic agitation at room temperature in a two-electrode system with the Ti foil acting as the working electrode and a Pt rod as the counter electrode, which were connected to the positive and negative terminals of a dc power supply respectively. The distance between the two electrodes was fixed at approximately 2 cm. The electrolyte for anodization was a mixture of ethylene glycol and water (90 wt %:10 wt %) with 0.5 wt % of ammonium fluoride. The anodization was carried out with the applied voltage of 50 V for 3 h. When the anodization process was completed, the samples were removed from the electrolyte, then rinsed with distilled water and dried under air blow. They were subsequently annealed in a muffle furnace at 500 °C for 3 h for crystallization. Silver was loaded on the surface of TiO_2NTs by the photodeposition method to achieve the TiO_2NTs/Ag. In this process, the TiO_2NTs samples were soaked into silver nitrate aqueous solutions with three different concentrations (0.1 M, 0.5 M and 1.0 M) for 2 h followed by UV-illumination for 2 h. Each sample is named according to the concentration of silver nitrate solution, i.e., TiO_2NTs/Ag-0.1 M, TiO_2NTs/Ag-0.5 M and TiO_2NTs/Ag-1.0 M. The amount of the photocatalyst for each experiment may be estimated from the volume of the photocatalyst, which is the multiplication of the substrate dimensions and the film thickness (2 cm × 2 cm × 2 μm).

3.2. Physicochemical Characterization

The physicochemical properties such as size, size distribution, surface morphology, crystalline phase, optical behavior of TiO_2NTs and TiO_2NTs/Ag were investigated by field emission scanning electron microscopy (FESEM) (AURIGA CrossBeam Workstation, Carl Zeiss, Germany), X-ray diffraction (XRD) (SmartLab X-ray diffractometer with Cu Kα radiation, Rigaku, Japan), and Ultraviolet-visible diffuse reflectance spectroscopy (UV-DRS) (UV-2600 UV-VIS Spectrophotometer, Shimadzu, Japan). The surface properties and chemical states of TiO_2NTs and TiO_2NTs/Ag photocatalysts before and after the photocatalysis reactions were carried out were studied using X-ray photoelectron spectroscopy (XPS) (PHI5000 Versa Probe II, ULVAC-PHI, Japan) at the SUT-NANOTEC-SLRI joint research facility, Synchrotron Light Research Institute. The monochromatic Al Kα X-ray (1486.6 eV) was used.

3.3. Photocatalytic and Recycle Experiments

Methylene blue (MB) was used as a representative organic pollutant. It is a traditional dye widely used in textile industries, thus forming a common ingredient in wastewater from such industries. It contaminates the aquatic environment. In addition, it can cause eye burn which might lead to a permanent injury to human eyes. Therefore, the removal or separation of MB from water is considered one of the most environmental challenges during recent years. An MB solution was prepared by mixing 1.2 mg of MB and 100 mL of distilled water at pH-1. The TiO_2NTs, TiO_2NTs/Ag (0.1 M, 0.5 M and 1.0 M) were used as photocatalysts for degradation of MB in the aqueous solution. The reaction was carried out under the 24-W UV-A lamp (high-pressure mercury lamp, λ = 365 nm). Every 30 min, 2 mL of MB solution was withdrawn to measure the MB concentration using the UV-1600 spectrophotometer. The photodegradation efficiency, indicating simply the fraction of MB that remains after a given time, is $\eta(\%) = [(C_0 - C_t)/C_0] \times 100$ where, C_0 and C_t are the concentration of MB at t = 0 s and any time t, respectively. To study the changes in the system after multiple photodegradation cycles, we carried out repeated trials under identical conditions. The photocatalysts were rinsed with water and dried under air blow after each trial.

4. Conclusions

In summary, the electrochemically anodizedTiO_2NTs and TiO_2NTs loaded with varying amounts of Ag (TiO_2NTs/Ag) were used as UV-driven photocatalysts for the degradation of an organic pollutant (MB) in aqueous solution. The TiO_2NTs possess the anatase phase and the size of TiO_2NTs are 90–120 nm in diameter and ~2 um in length. The photodegradation experiment indicated that theTiO_2NTs/Ag-0.5 M catalyst provided a photodegradation efficiency of 98% and degradation rate constant of 0.0138 min-1which are higher than those of pristine TiO_2NTs (83%, 0.0059 min^{-1}). This can be attributed to enhanced charge separation and higher reductive power in the presence of Ag, thereby suppressing charge recombination. The recycling experiment revealed that the PDE is diminished by 8.4% after eight runs of TiO_2NTs and by 18.4% after six runs of TiO_2NTs/Ag catalyst. The XPS surface analysis demonstrated that the physical origin of diminishing efficiency is a combination of carbon contamination and Ag leaching in recycled TiO_2NTs/Ag. The interesting finding was that the presence of silver on TiO_2TNs could reduce the accumulation of carbon contamination on the surface of TiO_2TNs. This suggests that a proper preparation method is required to decorate silver on TiO_2NTs to reduce a leasing rate in order to prolong the lifetime of the TiO_2NTs/Ag photocatalyst.

Author Contributions: Conceptualization, T.Z.O. and P.S.; methodology, T.Z.O.; validation, T.Z.O., P.S. and M.F.S.; formal analysis, T.H.M.W., N.C. and P.S.; investigation, T.H.M.W., N.C., T.Z.O. and P.S.; data curation, T.H.M.W. and P.S.; writing—original draft preparation, T.H.M.W.; writing—review and editing, M.F.S., T.Z.O., P.S.; visualization, T.H.M.W., P.S.; supervision, F.C.; project administration, T.Z.O. and P.S.; funding acquisition, F.C. and P.S. All authors have read and agreed to the published version of the manuscript.

Funding: This research received no external funding.

Acknowledgments: This work has been partially supported by the Research Network NANOTEC program of the National Nanotechnology Center of Thailand and Thailand Center of Excellence in Physics. F.C. acknowledges the Pearl River Talent Program (2019QN01L951).

Conflicts of Interest: The authors declare no conflict of interest.

References

1. Kong, J.; Song, C.; Zhang, W.; Xiong, Y.; Wan, Y.M.; Wang, Y. Enhanced visible-light-active photocatalytic performances on Ag nanoparticles sensitized TiO_2 nanotube arrays. *J. Superlattices Microstruct.* **2017**, *109*, 579–587. [CrossRef]
2. Sun, K.C.; Qadir, M.B.; Jeong, S.M. Hydrothermal synthesis of TiO_2 nanotubes and their application as an over layer for dye-sensitized solar cells. *RSC Adv.* **2014**, *44*, 23223–23230. [CrossRef]

3. Nyein, N.; Tan, W.K.; Kawamura, G.; Matsuda, A.; Lockman, Z. Anodic Ag/TiO_2 nanotube array formation in NaOH/fluoride/ethylene glycol eletctrolyte as a photoanode for dye-sensitized solar cells. *J. Nanotechnol.* **2016**, *27*, 355605. [CrossRef] [PubMed]
4. Carroll, J.P.; Panaitescu, E.; Quilty, B.; Wang, L.; Menon, L.; Pillai, S. Antimicrobial properties of highly efficient photocatalytic TiO_2 nanotubes. *J. Appl. Catal. B* **2015**, *176*, 70–75. [CrossRef]
5. Zhou, X.; Liu, N.; Schmuki, P. Photocatalysis with TiO_2 nanotubes: "colorful" reactivity and designing site-specific photocatalytic centers into TiO_2 nanotubes. *ACS Catal.* **2017**, *7*, 3210–3235. [CrossRef]
6. Liao, Y.; Brame, J.; Que, W.; Xiu, Z.; Xie, H.; Li, Q.; Fabian, M.; Alvarez, P.J. Photocatalytic generation of multiple ROS types using low-temperature crystallized anodic TiO_2 nanotube arrays. *J. Hazard. Mater.* **2013**, *260*, 434–441. [CrossRef] [PubMed]
7. Paramasivam, I.; Jha, H.; Liu, N.; Schmuki, P. A review of photocatalysis using self-organized TiO_2 nanotubes and other ordered oxide nanostructures. *Small* **2012**, *8*, 3073–3103. [CrossRef] [PubMed]
8. Ibukuna, O.; Jeonga, H.K. Tailoring titanium dioxide by silver particles for photocatalysis. *Curr. Appl. Phys.* **2020**, *20*, 23–28. [CrossRef]
9. Cheng, X.; Yu, X.; Xing, Z. Characterization and mechanism analysis of Mo–N-co-doped TiO_2 nano-photocatalyst and its enhanced visible activity. *J. Colloid Interface Sci.* **2012**, *372*, 1–6. [CrossRef]
10. Nazari, M.; Golestani-Fard, F.; Bayati, R.; Eftekhari-Yekta, B. Enhanced Photocatalytic activity in anodized WO3-loaded TiO_2 Nanotubes. *Superlattices Microstruct.* **2015**, *80*, 91–101. [CrossRef]
11. Zheng, X.; Zhang, D.; Gao, Y.; Wu, Y.; Liu, Q.; Zhu, X. Synthesis and characterization of cubic Ag/TiO_2 nanocomposites for the photocatalytic degradation of methyl orange in aqueous solutions. *J. Inorg. Chem. Commun.* **2019**, *110*, 107589. [CrossRef]
12. Ren, X.H.; Qi, X.; Shen, Y.Z.; Xiao, S.; Xu, G.H.; Zhang, Z.; Huang, Z.Y.; Zhong, J.X. 2D co-catalytic MoS2 nanosheets embedded with 1D TiO_2 nanoparticles for enhancing photocatalytic activity. *J. Phys. D* **2016**, *49*, 315304. [CrossRef]
13. Xia, L.; Bai, J.; Li, J.; Zeng, Q.; Li, X.; Zhou, B. A highly efficient BiVO4/WO3/W heterojunction photoanode for visible-light responsive dual photoelectrode photocatalytic fuel cell. *J. Appl. Catal. B* **2016**, *183*, 224–230. [CrossRef]
14. Qian, S.; Wang, C.; Liu, W.; Zhu, Y.; Yao, W.; Lu, X. An enhanced CdS/TiO_2 photocatalyst with high stability and activity: Effect of mesoporous substrate and bifunctional linking molecule. *J. Mater. Chem.* **2011**, *21*, 4945–4952. [CrossRef]
15. Yuan, Y.; Ruan, L.; Barber, J.; Chye, S.; Xue, C. Hetero-nanostructured suspended photocatalysts for solar-to-fuel conversion. *J. Energy Environ. Sci.* **2014**, *7*, 3934–3951. [CrossRef]
16. Zhu, J.; Yang, D.; Geng, J.; Chen, D.; Jiang, Z. Synthesis and characterization of bamboo-like CdS/TiO_2 nanotubes composites with enhanced visible-light photocatalytic activity. *J. Nanopart. Res.* **2008**, *10*, 729. [CrossRef]
17. Sahrin, N.T.; Nawaz, R.; Kait, C.F.; Lee, S.L.; Wirzal, M.D.H. Visible light photodegradation of Fromaldehyde over TiO_2 nanotubes synthesized via electrochemical anodization of titanium foil. *J. Nanomater.* **2020**, *10*, 128. [CrossRef]
18. Hou, W.; Cronin, S.B. A review of surface plasmon resonance-enhanced photocatalysis. *Adv. Funct. Mater.* **2013**, *13*, 1612–1629. [CrossRef]
19. Khan, M.M.; Ansari, S.A.; Amal, M.I.; Lee, J.; Cho, M.H. Highly visible light active Ag@TiO_2 nanocomposites synthesized using an electrochemically active biofilm: A novel biogenic approach. *RSC Nanoscale* **2013**, *5*, 4427–4435. [CrossRef]
20. Albiter, E.; Valenzueal, M.A.; Alfaro, S.; Valverde-Aguilar, G.; Martínez-Pallares, F.M. Photocatalytic deposition of Ag nanoparticles on TiO_2: Metal precursor effect on the structural and photoactivity properties. *J. Saudi Chem. Soc.* **2015**, *19*, 563–573. [CrossRef]
21. Kumar, R.; Rashid, J.; Barakat, M.A. Zero valent Ag deposited TiO_2 for the efficient photocatalysis of methylene blue under uv-c light irradiation. *Colloids Interface Sci. Commun.* **2015**, *5*, 1–4. [CrossRef]
22. Malik, P. Photodegradation of methylene blue by silver doped TiO_2 thin films. *Adv. Sci. Focus* **2013**, *11*, 301–305. [CrossRef]
23. Jin, B.; Zhou, X.; Xu, X.; Ma, L.; Wu, Z.; Huang, Y. C@Ag/TiO_2: A highly efficient and stable photocatalyst active under visible light. *J. Nano Sci. Eng.* **2013**, *3*, 1–5. [CrossRef]

24. Nainani, R.; Thakur, P.; Chaskar, M. Synthesis of silver doped TiO_2 nanoparticles for the improved photocatalytic degradation of Methyl Orange. *J. Mater. Sci. Eng. B* **2012**, *2*, 52–58.
25. He, Y.; Basnet, P.; Hunyadi Murph, S.E.; Zhao, Y. Nanoparticle embedded TiO_2 composite nanorod arrays fabricated by oblique angle deposition: Toward plasmonic photocatalysis. *ACS Appl. Mater. Interfaces* **2013**, *5*, 11818–11827. [CrossRef] [PubMed]
26. Yang, G.; Hu, P.; Cao, Y.B. Fabrication of porous TiO_2 hollow spheres and their application in gas sensing. *Nanoscale Res. Lett.* **2010**, *9*, 437–1441. [CrossRef] [PubMed]
27. Hirakawa, T.; Kamat, P.V. Charge separation and catalytic activity of Ag@TiO_2 core-shell composite clusters under UV-irradiation. *J. Am. Chem. Soc.* **2005**, *127*, 3928–3934. [CrossRef]
28. Banerjee, S.; Pillai, S.C.; Falaras, P.; O'shea, K.E.; Byrne, J.A.; Dionysiou, D.D. New insights into the mechanism of visible light photocatalysis. *J. Phys. Chem. Lett.* **2014**, *5*, 2543–2554. [CrossRef]
29. Kim, Y.; Hwang, H.; Wang, L.; Kim, I.; Yoon, Y.; Lee, H. Solar-light photocatalytic disinfection using crystalline/amorphous low energy bandgap reduced TiO_2. *Sci. Rep.* **2016**, *6*, 25212. [CrossRef]
30. Zielinska, A.; Kowalska, E.; Sobczakd, J.W.; Łacka, I.; Gazdac, M.; Ohtanie, B.; Hupka, J.; Zaleska, A. Silver-doped TiO_2 prepared by microemulsion method: Surface properties, bio- and photoactivity. *J. Sep. Purif. Technol.* **2010**, *72*, 309–318. [CrossRef]
31. Wu, Y.; Liu, Z.; Li, Y.; Chen, J.; Zhu, X.; Na, P. WS2 nanodots-modified TiO_2 nanotubes to enhance visible-light photocatalytic activity. *Mater. Lett.* **2019**, *240*, 47–50. [CrossRef]
32. Feng, C.; Li, G.; Ren, P.; Wang, Y.; Huang, X.; Li, D. Effect of photo-corrosion of Ag_2CO_3 on visible light photocatalytic activity of two kinds of Ag_2CO_3/TiO_2 prepared from different precursors. *Appl. Catal. B* **2014**, *158*, 224–232. [CrossRef]
33. Momeni, M.M.; Ghayeb, Y.; Gheibee, S. Silver nanoparticles decorated titanium dioxide-tungsten trioxide nanotube films with enhanced visible light photo catalytic activity. *Ceram. Int.* **2017**, *43*, 564–570. [CrossRef]
34. Sorathiya, K.; Mishra, B.; Kalarikkal, A.; Reddy, K.P.; Gopinath, C.S.; Khushalani, D. Enhancement in rate of photocatalysis upon catalyst recycling. *Sci. Rep.* **2016**, *6*, 35075. [CrossRef] [PubMed]
35. Li, Y.; Zhao, H.; Yang, M. TiO_2 nanoparticles supported on PMMA nanofibers for photocatalytic degradation of methyl orange. *J. Colloid Interface Sci.* **2017**, *508*, 500–507. [CrossRef] [PubMed]
36. Sarkar, A.K.; Saha, A.; Tarafdar, A.; Panda, A.B.; Pal, S. Efficient removal of toxic dyes via simultaneous adsorption and solar light driven photodegradation using recyclable functionalized amylopectin-TiO_2-Au nanocomposite. *ACS Sustain. Chem. Eng.* **2016**, *4*, 1679–1688. [CrossRef]
37. Saravani, A.Z.; Nadimi, M.; Aroon, M.A.; Pirbazari, A.E. Magnetic TiO_2/$NiFe_2O_4$/reduced graphene oxide nanocomposite as a recyclable photocatalyst for photocatalytic removal of methylene blue under visible light. *J. Alloys Compd.* **2019**, *803*, 291–306. [CrossRef]
38. Costa, L.L.; Prado, A.G.S. TiO_2 nanotubes as recyclable catalyst for efficient photocatalytic degradation of indigo carmine dye. *J. Photochem. Photobiol. A* **2009**, *201*, 45–49. [CrossRef]
39. Lee, K.; Lin, S.; Lin, C.; Tsai, C.; Lu, Y. Size effect of Ag nanoparticles on surface plasmon resonance. *Surf. Coat. Technol.* **2008**, *202*, 5339–5342. [CrossRef]
40. Amendola, V.; Bakr, O.M.; Stellacci, F. A study of the surface plasmon of silver nanoparticles by the discrete dipole approximation method: Effect of shape, size structure and assembly. *Plasmonics* **2010**, *5*, 85–97. [CrossRef]
41. Liu, Y.; Wang, Y.X.; Yang, F.; Yang, X. Excellent antimicrobial properties of mesoporous anatase TiO_2 and Ag/TiO_2 composite films. *Microporous Mesoporous Mater.* **2006**, *114*, 431–439. [CrossRef]
42. Sheng, J.; Xu, H.; Tang, C. Preparation and photocatalytic activity of Ag-Modified SnO_2 @ TiO_2 Core-Shell Composites. *J. Environ. Anal. Toxicol.* **2016**, *6*, 1000372. [CrossRef]
43. Ge, M.Z.; Cao, C.Y.; Li, S.H.; Tang, Y.X.; Wang, L.N.; Qi, N.; Huang, J.Y.; Zhang, K.Q.; Al-Deyab, S.S.; Lai, Y.K. In situ plasmonic Ag nanoparticle anchored TiO_2 nanotube arrays as visible-light-driven photocatalysts for enhanced water splitting. *Nanoscale* **2016**, *8*, 5226–5234. [CrossRef]
44. Yu, L.; Yang, X.; Ye, Y.; Peng, X.; Wang, D. Silver nanoparticles decorated anatase TiO_2 nanotubes for removal of pentachlorophenol from water. *J. Colloid Interface Sci.* **2015**, *453*, 100–106. [CrossRef]
45. Lian, Z.; Wang, W.; Xiao, S.; Li, X.; Cui, Y.; Zhang, D.; Li, G.; Li, H. Plasmonic silver quantum dots coupled with hierarchical TiO_2 nanotube arrays photoelectrodes for efficient visible-light photoelectrocatalytic hydrogen evolution. *Sci. Rep.* **2015**, *5*, 10461. [CrossRef] [PubMed]

46. Luan, X.; Wang, Y. Preparation and photocatalytic activity of Ag/bamboo-type TiO_2 nanotube composite electrodes for methylene blue degradation. *J. Mater. Sci. Semicond. Process.* **2014**, *25*, 43–51. [CrossRef]
47. Ma, J.; Yang, M.; Sun, Y.; Li, C.; Li, Q.; Gao, F.; Yu, F.; Chen, J. Fabrication of Ag/TiO_2 nanotube array with enhanced photo-catalytic degradation of aqueous organic pollutant. *Phys. E Low Dimens. Syst. Nanostruct.* **2014**, *58*, 24–29. [CrossRef]